Materials Science and Engineering B 273 (2021) 115390

Contents lists available at ScienceDirect

Materials Science & Engineering B

journal homepage: www.elsevier.com/locate/mseb

Complex pulse magnetization process and mechanical properties of spark plasma sintered bulk MgB_2

Muralidhar Miryala [a,*], Sai Srikanth Arvapalli [a], Naomichi Sakai [a], Masato Murakami [a], Hidehiko Mochizuki [b], Tomoyuki Naito [b], Hiroyuki Fujshiro [b], Milos Jirsa [c], Akira Murakami [d], Jacques Noudem [e]

[a] Materials for Energy and Environmental Laboratory, Superconducting Materials Group, Shibaura Institute of Technology, 3-7-5 Toyosu, Koto-Ku, Tokyo 135-8548, Japan
[b] Faculty of Science and Engineering, Iwate University, Morioka, 4-3-5 Ueda, Japan
[c] Institute of Physics ASCR, Na Slovance 2, Praha 8 18221, Czech Republic
[d] National Institute of Technology, Ichinoseki College, Ichinoseki, Iwate 021-8511, Japan
[e] CRISMAT-CNRS, ENSICAEN, Normandy University, Caen, France

A R T I C L E I N F O

Keywords:
MgB2
Spark plasma sintering
Pulse field magnetization
Critical current density
Mechanical properties

A B S T R A C T

High-density MgB_2 bulks with superior mechanical and superconducting properties were fabricated using spark plasma sintering (SPS). The sharp superconducting transition at 37.5 K proved high quality of the superconductors. Critical current density significantly exceeded that of conventionally sintered bulks. Flux pinning diagrams indicated dominance of grain boundary pinning, with peak position at 0.2. SPS bulks showed improved mechanical properties with 8-times higher bending strength compared to dense hot isostatic pressed bulks. Trapped field was measured at 14 K and 20 K, 1 mm above the bulk's surface, with applied pulse field up to 2 T. A local overheating together with a complex trapped field formation in the MgB_2 bulks during pulse-field magnetization were studied to elucidate limitations of Pulse Field Magnetization.

1. Introduction

Superconductivity in MgB_2 was discovered in 2001 [1]. It soon gained a huge attention because it brought a superconducting state different both from conventional metallic superconductors and the high-T_c ones, cuprates. It presented new challenges for superconductivity theory. Interesting was also its simple and cheap chemical structure. Although the intermediate critical temperature (around 37 K) is not competitive with high-T_c compounds, it is still much better than in metallic superconductors. For potential applications, one can work with cheaper alternative coolants to liquid He such as liquid H_2 (~20 K), liquid Ne (~27 K) or recently developed advanced cryocoolers. The conventional superconductors like Nb_3Sn ($T_c \sim 18$ K) and Nb-Ti ($T_c \sim 10$ K) used in most applications till now somewhat lose their appeal due to need to be operated at or below 4.2 K, boing point of liquid helium. Hence, superconducting materials such as MgB_2 and $REBa_2Cu_3O_y$ "REBCO" (RE: Y, Nd, Sm, Gd, Eu) have become a new point of interest. Apart from the magnet applications such as NMR, MRI, water cleaning etc., MgB_2 superconductor has potential uses in superconducting transformers, rotors, magnetic drug delivery, space applications, transmission cables etc. [2–6]. The competing REBCO has a huge advantage over MgB_2 in T_c, however it has severe issues like weak-links at grain boundaries, a long processing time, expensive precursors, and inability to be used as powder-in-tube technology (PIT). In order to tackle these issues, research suggested solutions such as single-grain growth using melt growth (MG) and/or infiltration growth (IG), post-oxygenation etc., which all consume huge amount of time. On the other hand, the absence of weak links at grain boundaries of bulk MgB_2 superconductors ensures that they do not need to be single-grain and can be fabricated by just sintering [7]. Due to the low T_c, the operating temperatures of Nb_3Sn and Nb-Ti superconductors are extremely low and flux jumps have been observed several times [8]. While the critical current densities, J_c, at respective operating temperatures of these superconductors are comparable, MgB_2, due to the low weight, possesses a clear advantage e.g. in space applications as well as in various motors for all-electric cars or planes [2]. Another class of superconductors are the

* Corresponding author.
E-mail address: miryala1@shibaura-it.ac.jp (M. Miryala).

https://doi.org/10.1016/j.mseb.2021.115390
Received 29 January 2021; Received in revised form 11 June 2021; Accepted 5 August 2021

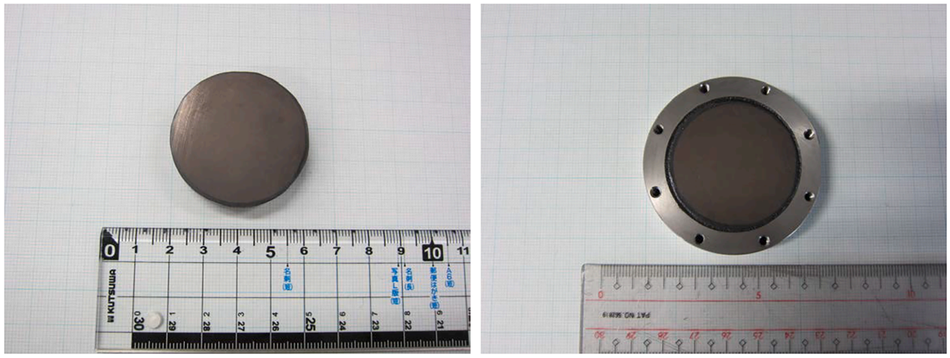

Fig. 1. Spark Plasma Sintering MgB_2 bulk with dimensions (left) and the bulk with Hastelloy support ring (right).

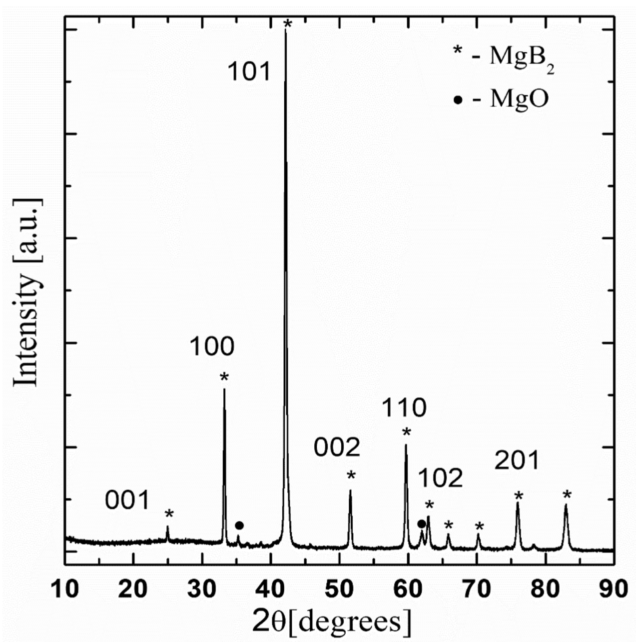

Fig. 2. Normalized X-ray diffraction pattern of SPS processed MgB_2 bulk.

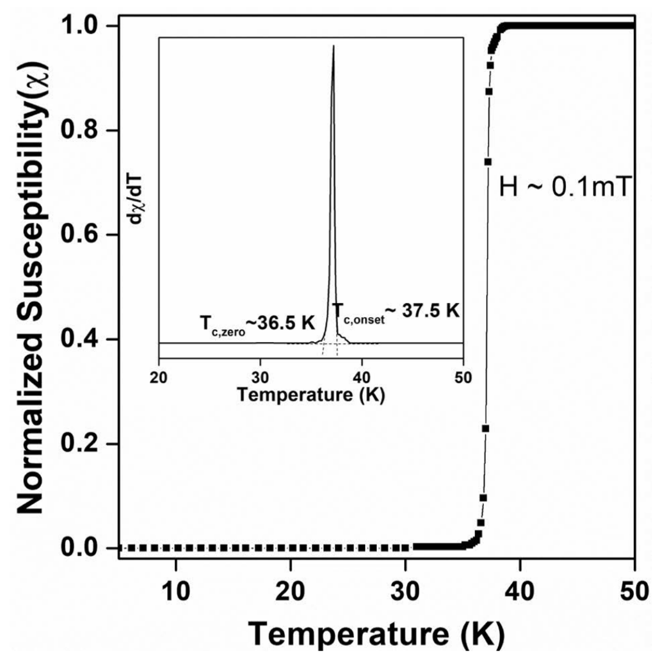

Fig. 3. DC susceptibility vs temperature of SPS processed MgB_2 bulk.

iron based superconductors, pnictides, that are very intriguing due to their non-BCS superconductivity as well as tunable T_c with chemical substitution. Their T_c ranges from 25 to 55 K, it is thus comparable to MgB_2, also J_c is decent. However, majority of these superconducting compounds involves Arsenic, which is volatile and highly toxic and makes them hard to deal with [9]. There have been studies of arsenic-free iron-based superconductors, their properties were, however, rather bad [10]. On the other hand, MgB_2 doesn't pose such problems and is easy to handle and fabricate.

Sintering of bulk MgB_2 is commonly carried out at ambient pressure. The bulks exhibit a good trapped magnetic field with a simple peak. In previous trials, excellent trapped field (TF) values of 1.5–3 T were reported in sintered bulk MgB_2 superconductors (diameter 20–30 mm) [11–13]. Recent research showed that the MgB_2 bulk magnet due to its uniform TF as well as low decay is a promising candidate for the magnetic pole in NMR [13]. The authors demonstrated the use of MgB_2 magnet to detect the ^{1}H nuclear magnetic resonance. Moreover, it is well known that trapped magnetic field is directly proportional to bulk diameter. While fabrication of large single-grain REBCO bulks is difficult to due to the tedious multi-nucleation, this task is not difficult for polycrystalline MgB_2 bulks as the sintering process is simple and tunable. Due to this advantage, MgB_2 is commercially very attractive and intricate shapes and sizes can be easily fabricated, for example as magnetic shielding cups for circular proton colliders etc. [14]. Only, the mechanical properties of bulk MgB_2 superconductors fabricated by sintering under the ambient pressure are not as good as in bulk REBCO superconductors [13,14]. In addition, there are some other issues such as high porosity (low packing ratio), low H_{c2} and weak flux pinning. Moreover, it is known from prior research that bulk superconductors experience thermal stresses when subjected to electromagnetic force [15,16]. Improved mechanical properties of the bulk can thus enhance trapped magnetic field. Fabrication techniques such as hot isostatic pressing (HIP) and spark plasma sintering (SPS) result in high packing ratio in bulk MgB_2 and thus they are good technology candidates for improving trapped field properties [15–19]. SPS is robust and fast technique capable of producing high-density (high packing ratio) MgB_2 bulks, just what required in this system. With SPS, it is possible to obtain very high densities, up to 99 %. This technique enables control over pressure and temperature in various time frames. Complicated heating patterns can be executed. In the case of MgB_2, Mg reacts with boron leaving pores behind; it requires high pressure to close these pores as the reaction proceeds. Such technique needs optimization for obtaining best performance bulk MgB_2. In the present work we display the enhanced properties of SPS prepared bulk MgB_2 specimens compared to other techniques, especially hot-isostatic pressing (HIP) by pressures of 98 and 196 MPa at 900 °C for 3 h resulting in packing fractions of 63 and 92 % [15].

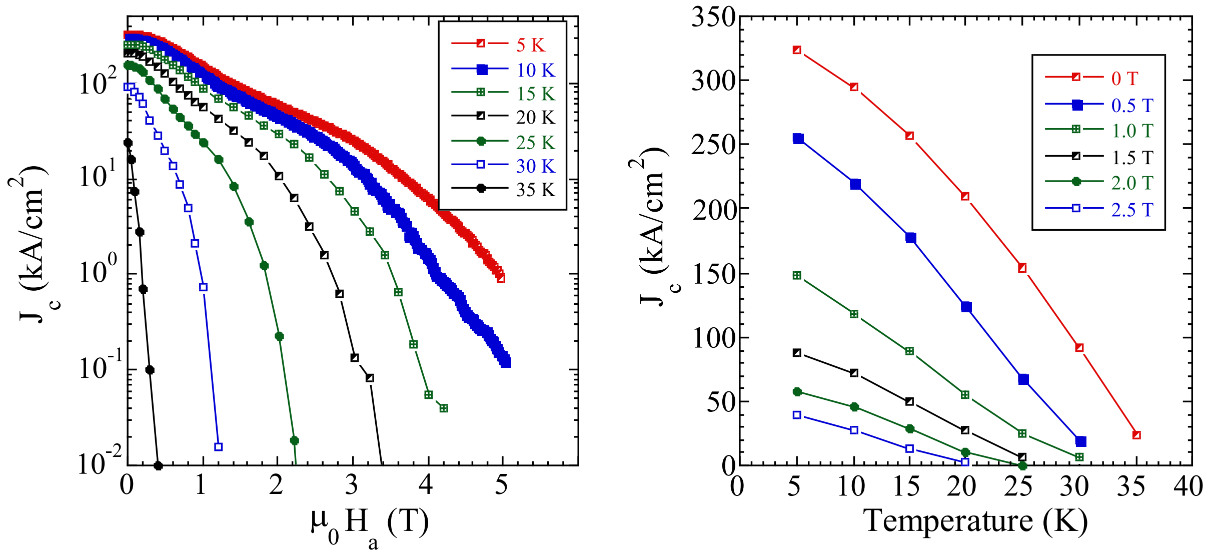

Fig. 4. Critical current densities of SPS MgB_2 bulk at various temperatures (5–35 K) and fields (0–5 T).

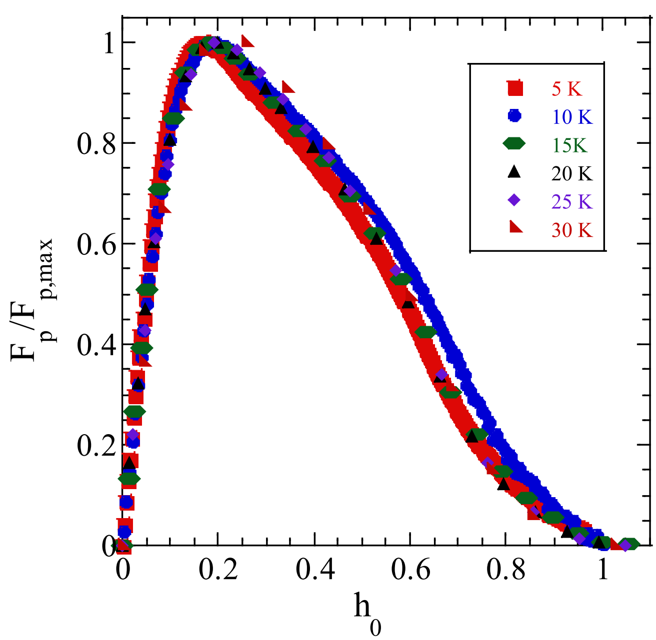

Fig. 5. Flux pinning diagrams of SPS MgB_2 bulk at various temperatures. At all temperatures, the peak position is 0.2.

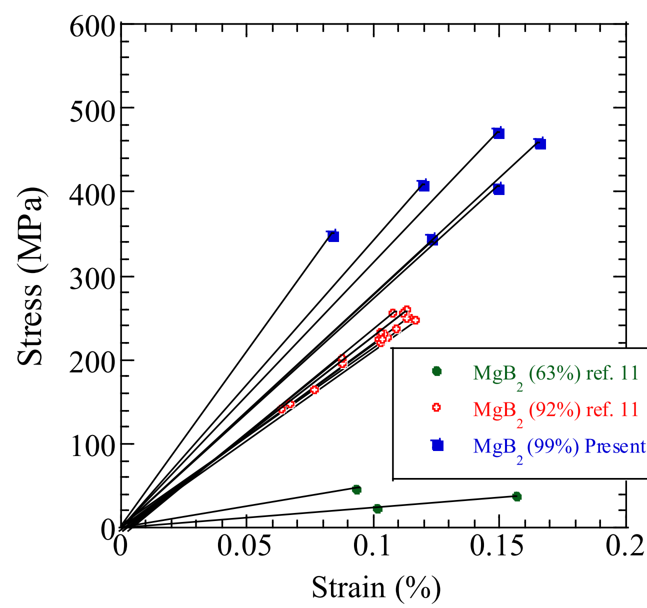

Fig. 6. Stress – strain curves of the current SPS MgB_2 specimen in comparison with previous highly dense bulks.

2. Experimental

1) Bulk fabrication:

The commercial MgB_2 powder from ABCR GmbH (Karlsruhe, Germany) was used as a precursor. SPS was applied at 1150 °C under pressure of 50 MPa for 20 min and alternatively in vacuum of 10^{-2} Pa. The pulsed electric current of 2 kA was used to heat the sample. A graphite die of 40 mm diameter was used to prepare bulk samples about 10.5 mm thick. Soon after sintering, the bulk samples were polished to remove the graphite coating (see Fig. 1, left). Details of the SPS process and superconducting properties of a spark plasma sintered bulk MgB_2 piece were reported elsewhere [19]. The bulks were later characterized using X-ray diffraction (XRD- Smart lab/Rigaku) to confirm the single-phase state and atomic force microscopy (AFM) to see the microstructural modifications upon employing SPS technique.

2) Mechanical properties:

Mechanical properties of bulk MgB_2 superconductors processed by SPS were evaluated via bending tests. Three cuboidal specimens ($2.8 \times 2.1 \times 2.1$ mm^3) were cut from various locations of the bulk MgB_2 samples by a wire electric-discharge cutting machine. These specimens were subjected to 3-point bending test at room temperature. The force was applied along thickness in 0.2 mm/min speed by a crosshead using the SHIMADZU AG-50KNE testing machine. To record the strain, a strain gauge (0.2 mm in length) was attached to the surface experiencing tensile force. The 3-point bending stress σ was calculated using relation

$$\sigma = (M/I) \times (t/2) = 3PL/(2wt^2) \quad (1)$$

where M is bending moment, I is moment of inertia, P is applied load, L is outer supporting span (21 mm), w and t are width (2.8 mm) and thickness (2.1 mm) of the specimen, respectively.

3) Superconducting properties:

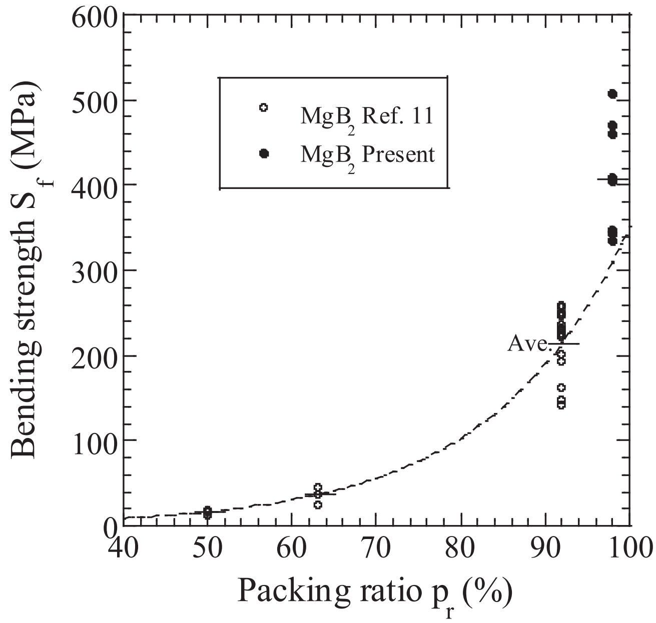

Fig. 7. Bending strength plotted against packing ratio of current SPS MgB_2 specimens in comparison with previous highly dense bulks.

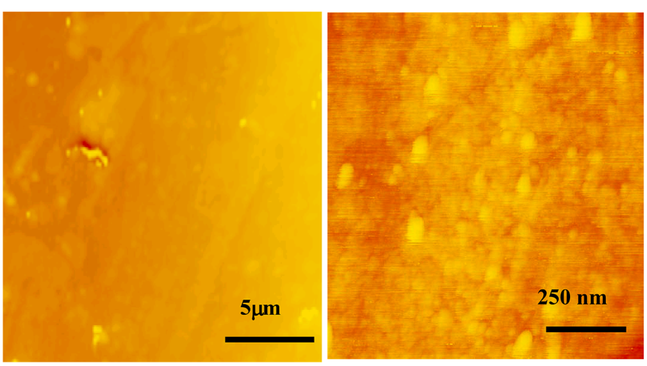

Fig. 8. Microstructure of SPS MgB_2 bulk studied by AFM. Almost zero porosity can be seen.

To reduce temperature rise and to reinforce mechanically the bulk, SUS304 ring was fixed on the 40 mm in diameter bulk MgB_2 before the trapped field experiment (see Fig. 1, right). The bulks were magnetized using pulse field magnetization (PFM) technique. The bulk was placed on a soft iron yoke with dimensions of 40 mm diameter and 20 mm thickness, which was tightly attached to the cold stage of a Gifford–McMahon (GM) cycle helium refrigerator. The sample space was later evacuated using an oil diffusion pump. Totally, three Hall probes were attached on the sample surface for a careful measurement, one at the center, one close to the edge, and one outside the surface. During the PFM, the time dependence of the local magnetic field at the center of the bulk surface was measured by Hall sensor connected to an oscilloscope. The total trapped magnetic flux was measured using an axial Hall sensor, which scanned stepwise on the vacuum chamber 5 mm above the bulk surface with a pitch of 1.2 mm. Temperature on the bulk surface was measured using a fine thermocouple.

3. Results and discussion

Fig. 2 depicts the diffraction pattern of the bulk using XRD, all the peaks belong to the MgB_2 phase, with only a few low peaks belonging to MgO phase. This confirms the formation of MgB_2 single phase along with scarce MgO impurities that are unavoidable and generally observed in this system. The superconducting critical transition temperature (T_c) was measured using SQUID magnetometer in magnetic field of 10 Oe. Fig. 3 depicts the normalized susceptibility vs. temperature. $T_{c,onset}$ was around 37.5 K, while $T_{c,zero}$ was close to 36.5 K. The critical transition width was around 1 K, a sharp transition telling us that the bulk was of high quality. In general, this value might be affected by a scarce MgO formation and by contaminations of commercial Mg and B powders. These values are similar to conventionally sintered MgB_2, indicating that SPS does not deteriorate sample quality [20]. The critical current density (J_c) was calculated from M−H curves obtained by SQUID measurements using the extended Bean critical state model [21], which reads

$$J_c = 20\Delta m/\left[a^2c\ (b - a/3)\right] \tag{2}$$

where a, b are cross sectional dimensions, $b > a$, and c is thickness of the specimen (a, b, c usually around 1, 1, 0.7 mm, respectively) and Δm (in emu units, 1 emu = 10^{-3} Am^2) is the difference of magnetic moments during decreasing and increasing field in the M-H loop. Superconducting performance was tested at a series of temperatures covering the entire superconducting range of the material, 5, 10, 15, 20, 25, 30, and 35 K (see Fig. 4 left). In addition, J_c as a function of magnetic field is discussed, in particular to analyze the high field performance. Self-field J_c values of 320, 300, and 260 kA/cm^2 were observed at 5, 10, and 15 K respectively. These values are slightly higher compared to conventional regularly sintered MgB_2. Fig. 4 right, displays J_c of the SPS bulk sample at various temperatures and fields. It shows that the bulks can be used in applications at 5, 10, 15, and 20 K up to 2, 1.5, 1, and 0.5 T, respectively.

Flux pinning diagrams in general are used to indicate the prevailing pinning mechanism. The results were evaluated in terms of Dew-Hughes general expression [22]

$$f_p = A(h)^p(1 - h)^q \tag{3}$$

where A is a constant, f_p is normalized flux pinning force, $f_p = F_p/F_{p,max}$, and h is reduced magnetic field, $h = H/H_{irr}$, where the irreversibility field, H_{irr}, was determined as the field, where J_c in the $J_c(H)$ dependence fell down to 100 A/cm^2, a standard practice in our works. The $f_p(h)$ dependence was analysed at 20 K. Dew-Hughes model correlates the peak position of the normalized pinning force density vs. magnetic field normalized to B_{c2} (or B_{irr}) with different types of pinning regimes in the material. For example, peak position at 0.2 implies grain boundary pinning, at 0.33 implies δT_c pinning and 0.5 indicates point pinning. The peak shifts to the right if the J_c at high magnetic fields is improved, i.e. if there are effective high-field pinning centers. MgB_2 superconductor studied here is a bulk granular system. Microstructure studies show a typical grain size of a few hundred nm to a few micrometers. In cuprate bulks grain boundaries are weak links preventing flow of large critical currents over the sample. Thus, cuprate bulks have to be single-crystals to exhibit high critical currents. Grain boundaries in MgB_2 are strong links allowing for a free flow of currents over the entire bulk. Taking the low anisotropy of the MgB_2 into consideration, the polycrystalline. From electromagnetic point of view, the polycrystalline MgB_2 bulk behaves like a single-crystal, which is unique. From structural point of view, grains in the MgB_2 bulk still exist and play role of effective large defects [23]. It is consistent with the pinning diagram indicating peak position around 0.2 in all MgB_2 samples. Additives of various kinds trying to induce some sort of nm-sized point-like defects in MgB_2 samples [24] change the pinning diagram only a little, proving that the principal pinning mechanism in MgB_2 is boundary pinning as in Fig. 5.

Fig. 5 shows that in our case $h_{max} \sim 0.2$, consistently for various temperatures, 5, 10, 15, 20, 25, 30, 35 K. This indicates that the dominant pinning mechanism is associated with grain boundaries, as in our prior bulk MgB_2 systems [25–27]. A slight shift of h_{max} towards higher fields can be seen with increasing temperature, which is due to temperature dependence of inherent effective mass anisotropy, γ (which decreases) [28]. In addition, a shoulder on the right part of the curve

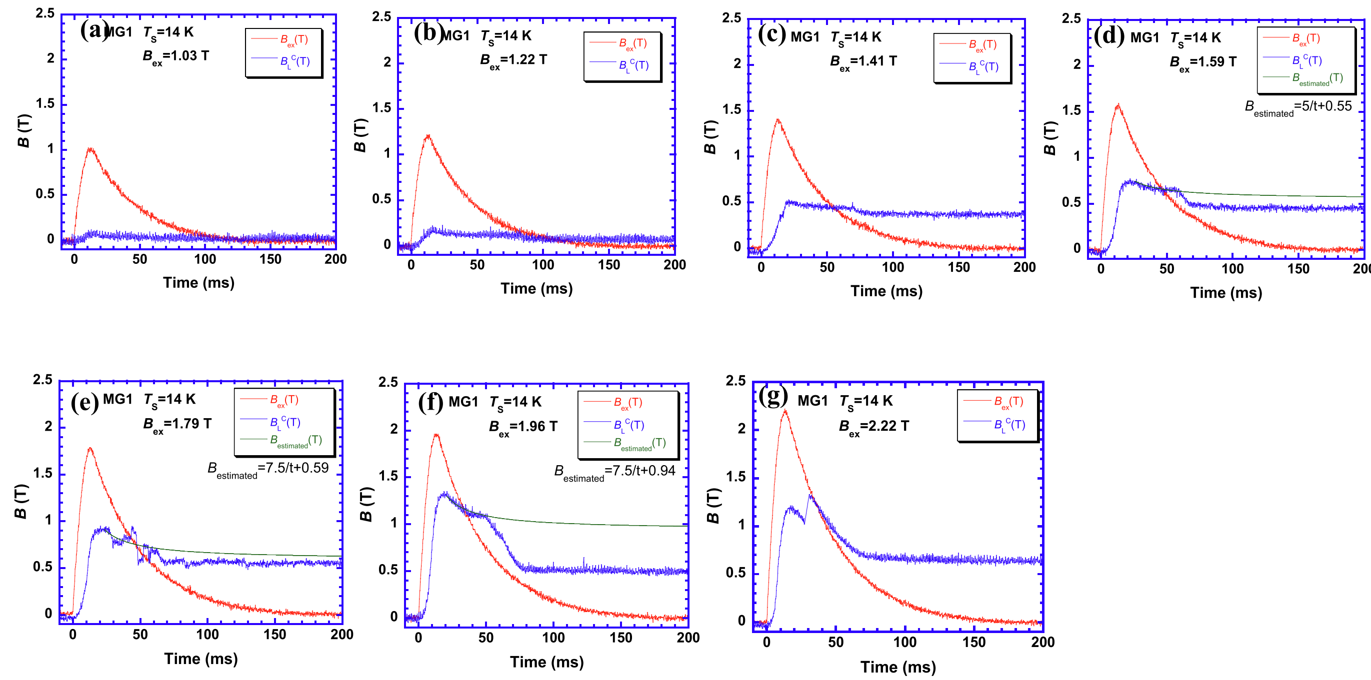

Fig. 9. Time evolution of the applied field (B_{ex}) and local field (B_L^C) at the center of bulk surface at 14 K. a, b, c, d, e, f, and g correspond to B_{ex} = 1, 1.2, 1.4, 1.6, 1.8, 2, and 2.2 T, respectively.

appears, indicating an improved J_c at high fields. This shape implies that grain boundaries are the principal pinning mechanism but there is also a weak effect of point-like pins, effective at higher magnetic fields. This point requires a further study.

In the present work, we used the sintering temperature of 1150 °C for SPS bulk MgB_2, significantly higher than 800 °C found as optimum reaction temperature for conventional sintering. It is well know that a higher reaction temperature favors grain growth and agglomeration that result in growth of large grains associated with a lower grain boundary density [29]. We believe that the heat cycle of SPS process can be optimized to obtain highly dense bulks with small grains and a higher grain boundary density.

As we deal with a brittle granular system, we need in addition to good superconducting properties also decent mechanical properties. Especially, when targeting high TF superconducting magnets, we need sufficient mechanical strength to sustain the considerable Lorentz forces during magnetization up to certain fields. For trapping magnetic fields higher than 7–8 T, a special stainless-steel ring reinforcement is needed [30]. Fig. 6 depicts the stress–strain curves of various specimens cut from the SPS bulk. The curves show a linear stress–strain dependence until the fracture point in bulks with both high and low packing fraction (99, 92 and 63 %). However, sometimes a non-linear behavior could be observed in low packing fraction bulks, which could occur due to the slow propagation speed of cracks while loading [15]. The fracture stress of the present SPS bulks with 99% packing fraction is around 330–480 MPa, while those of the dense bulks prepared by A. Murakami *et al.* [15], with 92% and 63% packing fraction (via hot isostatic pressing "HIP"), were around 220 and 50 MPa on average, respectively. This points out to the brittleness and ceramic nature of the high-density MgB_2 bulk specimens. In addition, the slopes of the slope of stress-strain curves i.e.Young's modulus, is high for high density/packing fraction bulks. As seen in Fig. 7, the less dense samples with a lower packing fraction have low bending strengths. The average bending strength of the present SPS bulks is around 410 MPa, while that of prior HIP high dense bulk with 92% packing fraction was around 200 MPa. On the other hand, the bending strengths of HIP low dense sample with 63% packing fraction and reference bulk with 50% packing fraction were around 50 and 10 MPa, respectively. The bending strengths of current bulk is almost 8 times that of HIP processed bulk. The bending strength increases with increasing packing ratio, which rises with the SPS temperature. This bending strength improvement is due to the increase of the net cross-sectional area and material density of the bulk caused by the increase of the packing ratio compared to regular sintering where the net cross-sectional area is very low due to 50% porosity. In addition, reduction of stress concentration centers (especially defects, voids etc.) in the matrix together with the increase of packing ratio also contributes to the improvement of the bending strength. The bending strength results did not vary with the loading direction of the specimen (parallel or perpendicular to thickness), which points out that matrix of the SPS specimens is isotropic and uniform. The isotopic bending strength relates to Young's modulus, which also does not change with the loading direction [31]. As regards the isotropic behavior of the anisotropic material, we have to bear in mind that the tested bulk is polycrystalline. In such a sample, we can expect that mechanically weakest is the intergranular space. If the used technology enables preparation of a denser material (with respect to the reference, which possesses huge porosity and only 50% of the theoretical density), then the increased density appears naturally in the inter-grain space, which is isotropic on macroscopic scale. No wonder that bending strength is isotropic, too. The mechanical strength testing is not about individual MgB_2 grains, however about a macroscopic system of arbitrarily oriented MgB_2 grains. While MgB_2 compound is slightly anisotropic, its polycrystalline bulk system as a whole is isotropic. One important point to note is that high SPS sintering temperature enables high density. However, if we want to reduce the sintering or fabricating temperature (to maintain fine grain structure by avoiding grain coalescence), we have to increase pressure. It demands use of expensive dies capable of withstanding the high pressure, which reduces commercial viability. Therefore, one needs to compromise the parameters to get an optimized final product. To find the optimum, we studied the microstructure of the SPS bulk specimens using AFM. Fig. 8, left shows AFM images taken after polishing. One can see a highly dense MgB_2 material without pores. In higher magnification (Fig. 8, right), we tried to see the grain size distribution playing a crucial role in improving the critical current density. Note that the size of the

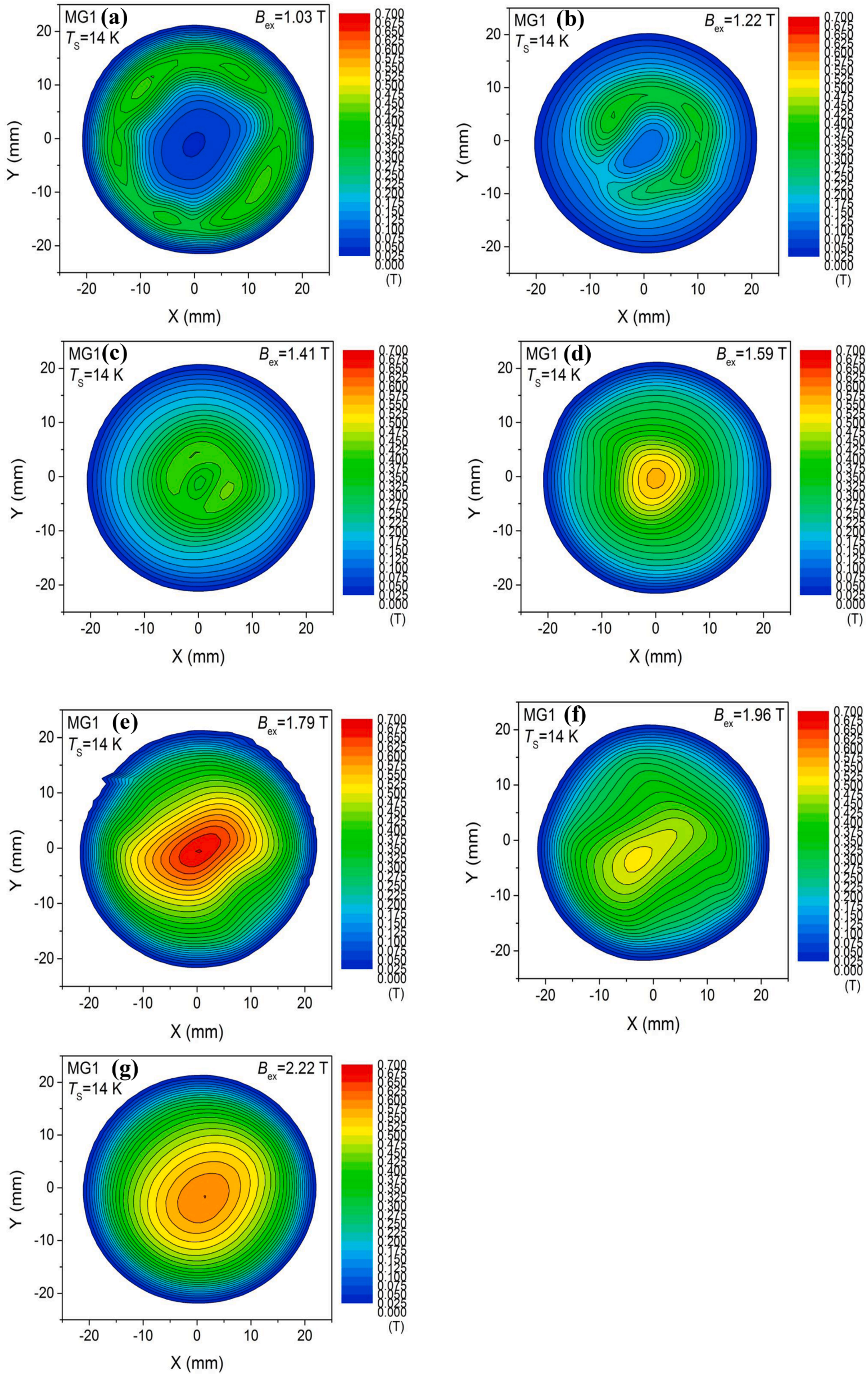

Fig. 10. Trapped field profiles of the SPS MgB_2 bulk mapped 1 mm above the surface at 14 K for various applied fields. a, b, c, d, e, f, and g correspond to B_{ex} = 1, 1.2, 1.4, 1.6, 1.8, 2, and 2.2 T, respectively.

MgB_2 grains is around 50–100 nm. In bulk MgB_2 material the grain size plays a crucial role in improving critical current density since the grain boundary pinning is dominant and the grain boundary density increases with grain size reduction. The smaller the grain size, the higher is critical current density and trapped field [32]. The suppression of porosity resulted in increase in J_c, as the superconducting volume per unit volume was now higher than before.

As high critical current density enhances trapped field (TF), we studied TF performance of the SPS bulks. Pulse field magnetization (PFM) was used to magnetize the bulk. The bulk's dimensions were

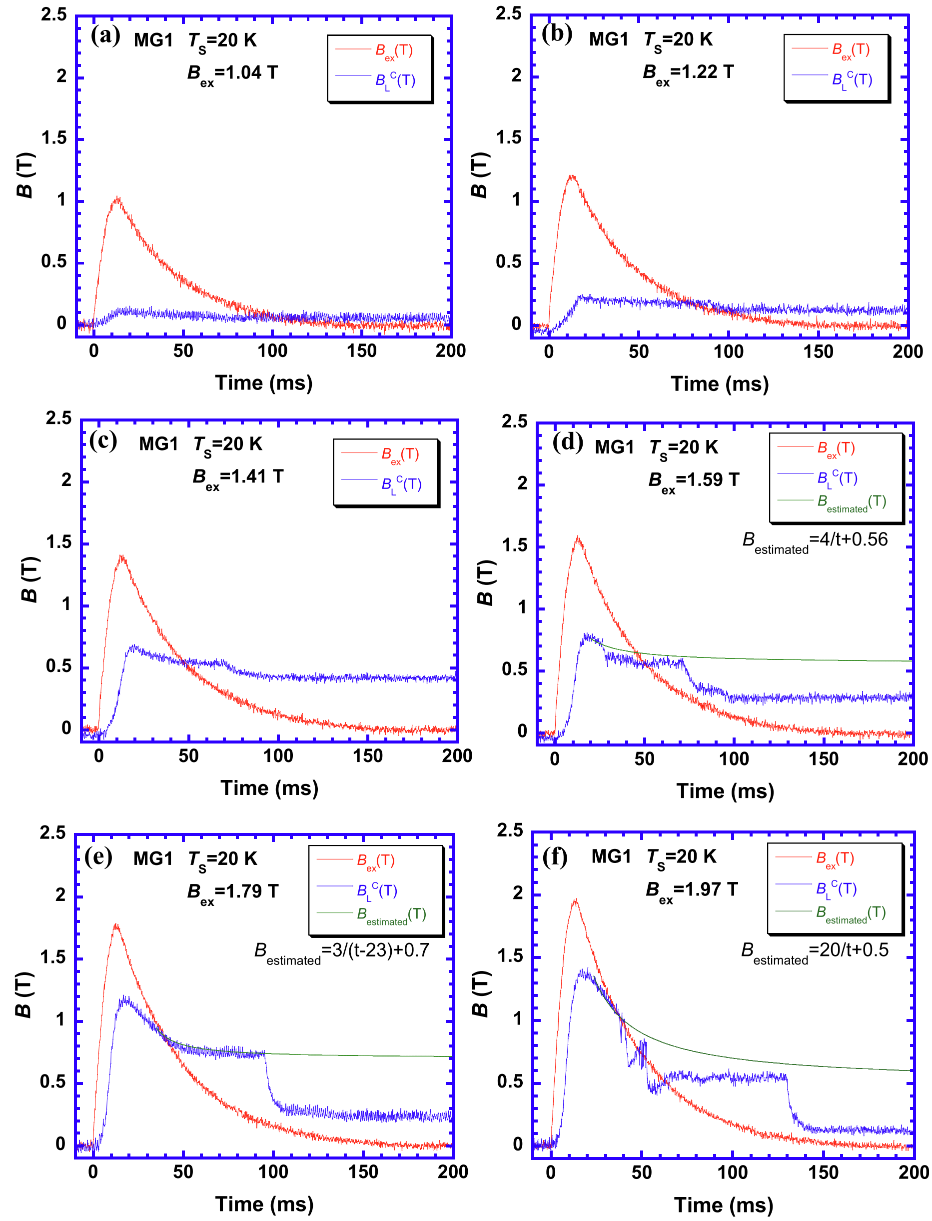

Fig. 11. Time evolution of the applied field (B_{ex}) and local field ($B_L{}^C$) at the center of bulk surface at 20 K. a, b, c, d, e, and f correspond to B_{ex} = 1, 1.2, 1.4, 1.6, 1.8, and 2 T, respectively.

around 40 mm diameter and 9.5 mm thickness. The packing fraction measured by Archimedes method was around 99.8%. The TF measurement was done after a sequence of increasing external magnetic fields (B_{ex}) from 1 T to 2.2 T in steps of 0.2 T at 14 K and later 1 T to 2 T in steps of 0.2 T at 20 K. All the TF data presented were measured at 5 mm above the sample surface.

The pulsed external field $B_{ex}(T)$ was applied as shown in the Fig. 9 (a–g), while the local trapped field $B_L{}^C(T)$ was measured at 14 K and the results are following.

i) With B_{ex} = 1 and 1.2 T, there was no significant local trapped field (Fig. 9 (a, b)) compared to the applied field. However, trapped field linearly increased up to the peak B_{ex}, and then remained constant at around 0.2 T.

ii) When B_{ex} = 1.4 T (Fig. 9 (c)), local TF raised up to 0.5 T and stood constant there. In fact, there was a slight drop in trapped field, commonly observed in MgB_2 bulk system. The reason is not yet clear, but it has been observed in many other works [33].

iii) When B_{ex} > 1.6 T, the bulk started to exhibit flux jumps, and hence we plotted estimated TF ($B_{estimated}$), calculated as $B_{estimated} = a/t + b$, where t - time; a,b – constants. At B_{ex} = 1.6 T, local TF was initially around 0.7 T, until a sudden flux drop occurring after a minute (Fig. 9 (d)). The local TF then stabilized at 0.5 T. Since there is sudden drop in the TF, we added the estimated curves to simulate the TF behavior without flux drop, via extrapolation. In this case, the extrapolation resulted in the relation $B_{estimated} = 5/t + 0.55$ and can be used as a reference.

iv) With B_{ex} = 1.8 and 2 T, the initial local TF was around 0.9 and 1.3 T, respectively. In Fig. 9 (e) we can see flux drops as well as irregular fluctuations and in Fig. 9 (f) there are two flux drops (initially small one, then a larger one). In both cases, the trapped field finally reached a constant value 0.5 T. The estimated TF curves were $B_{estimated} = 7.5/t + 0.59$ and $B_{estimated} = 7.5/t + 0.94$ for B_{ex} = 1.8 and 2 T, respectively.

v) When B_{ex} = 2.2 T (Fig. 9 (g)), there was an interference of the flux flow due to the large temperature rise with the dynamic motion of the magnetic flux (flux jump) at t = 25 ms. In the end, the TF value reached 0.7 T with a slow decrease resembling characteristic TF decay in MgB_2

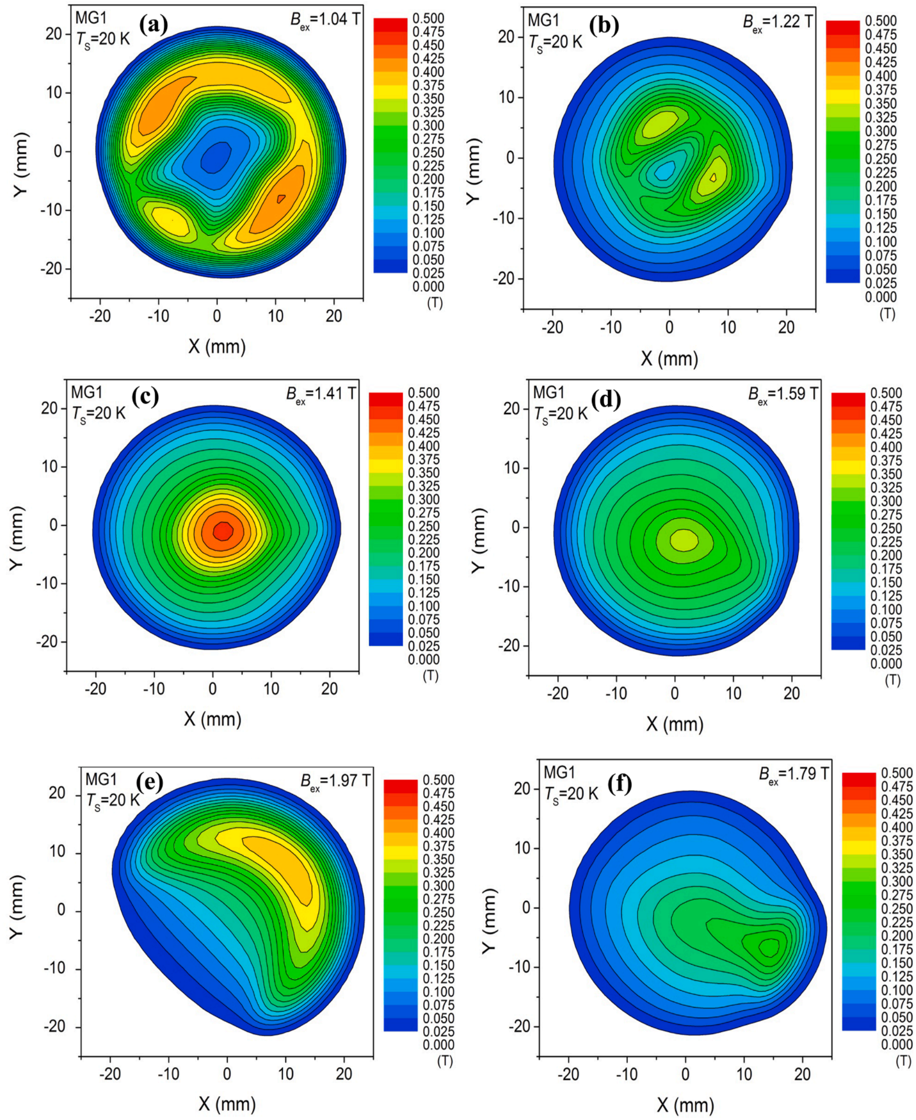

Fig. 12. Trapped field profiles of the SPS MgB_2 bulk mapped 1 mm above the surface at 20 K for various applied fields. a, b, c, d, e, f, and g correspond to $B_{ex} = 1$, 1.2, 1.4, 1.6, 1.8, and 2.2 T, respectively.

($t = 30$ to 60 sec).

To conclude this part, the maximum local TF in the bulk magnetized at 14 K saturated at 0.7 T. TF profiles mapped 1 mm above the bulk surface (Fig. 10 (a-g)) give more consistent results. At low applied fields ($B_{ex} = 1$, 1.2, and 1.4 T) the profiles showed a M−shaped TF distribution due to a partially magnetized state of the bulk [34–36]. In the applied fields 1.6 and 1.8 T, the TF profiles showed perfect uniform cone with TF increasing with applied field increment. In $B_{ex} = 2$ T, TF dropped maintaining still a uniform cone shape. It resembled an over-magnetized state of bulk. In $B_{ex} = 2.2$ T, the bulk showed a high TF with a uniform cone shape resembling the fully magnetized state of bulk.

The same experiments as at 14 K was repeated at 20 K (the common operating temperature for MgB_2 superconductors).

i) With $B_{ex} = 1$ and 1.2 T, there was a small local trapped field, increasing with B_{ex} up to pulse peak, and TF reached 0.1 and 0.3 T, respectively, and remained constant as shown in Fig. 11 (a,b).

ii) With $B_{ex} = 1.4$ T (Fig. 11 (c)), local TF first grew up to 0.6 T and then dropped slowly from $t = 20$ ms up to $t = 70$ ms, resembling thus the characteristic TF decay observed in most MgB_2. The latter consisted of a slight sudden flux loss at t = 70 ms followed by stabilization on 0.5 T.

iii) With $B_{ex} = 1.6$ and 1.8 T, the bulk showed a characteristic decay (Fig. 11 (d, e)) followed by flux drops at t = 70 ms and t = 100 ms. The local TF of the bulk increased upto around 0.7 and 1.2 T followed by drop and reached saturation on 0.3 T for both $B_{ex} = 1.6$ and 1.8 T. The extrapolated reference curves for $B_{ex} = 1.6$ and 1.8 T are $B_{estimated} = 4/t + 0.46$ and $B_{estimated} = 3/(t\text{-}23) + 0.7$ respectively. Figures show that the flux flow out or flux losses are very high, probably due to a large temperature increase caused by a rapid movement of the magnetic flux. On the other hand, at 14 K such large local TF drops were absent because at low operating temperature flux pinning was high and did not allow for a fast flux movement.

iv) With $B_{ex} = 2$ T (Fig. 11 (f)), a similar behavior as with $B_{ex} = 1.6$ and 1.8 T but much more violent and resulted in the very low final TF value saturated at 0.2 T as compared to the extrapolation, $B_{estimated} = 20/t + 0.5$. However, a peak TF of 1.4 T was observed until the flux flow.

The TF profiles were then also mapped 1 mm above the bulk surface at 20 K (Fig. 12 (a - f)). Similarly as in 14 K, at low applied fields ($B_{ex} = 1$ and 1.2 T) the TF profiles showed a uniform M−shaped TF distribution corresponding to a partially magnetized state. In moderate applied fields ($B_{ex} = 1.4$ and 1.6 T), the TF profiles showed a perfect cone shape. Only, the TF value for $B_{ex} = 1.6$ T was lower than for $B_{ex} = 1.4$ T. This showed that the sample was in over-magnetized and in fully magnetized state, respectively. In $B_{ex} = 1.8$ and 2 T, the TF profile showed distorted single

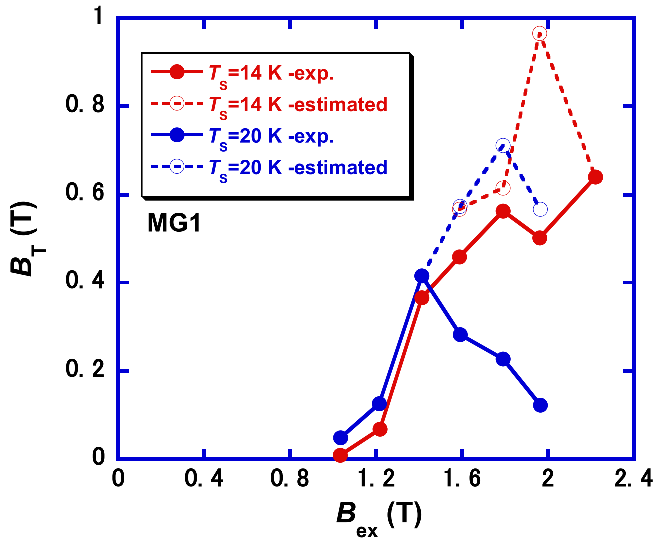

Fig. 13. Local trapped field at the center of the bulk surface and the model trapped field as a function of the applied pulse field at 14 and 20 K.

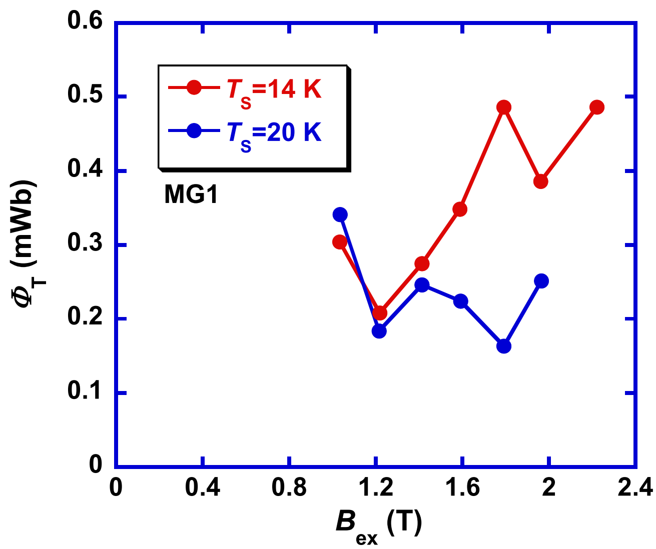

Fig. 14. Dependence of the total trapped flux (ϕ_T) 1 mm above bulk's surface on applied field at 14 and 20 K.

cones, probably due to flux jumps. When applying a large external magnetic field, moreover too fast, the material sometime cannot accommodate the critical state, the critical current density locally exceeds its maximum, and the material at that point loses superconducting nature locally, nonzero local resistivity causes a local overheating and critical current reduction appears in the form of so-called flux jumps.

Fig. 13 shows plot of the experimental and model local trapped field at the center of bulk surface as a function of B_{ex} for 14 K and 20 K. The highest local trapped field at 14 K was $B_T = 0.64$ T (for $B_{ex} \sim 2.2$ T), at 20 K $B_T = 0.42$ T (for $B_{ex} \sim 1.4$ T). The highest model trapped field was $B_{estimated} = 0.97$ T (for $B_{ex} \sim 2$ T) at 14 K and $B_{estimated} = 0.71$ T (for $B_{ex} \sim 1.8$ T) at 20 K. The lower operation temperature showed better performance and a shift of the B_T peak to higher applied fields. This was a consequence of increase in J_c, in pinning force, and in magnetic flux shielding. The TF values lowered or dropped before than estimated at $B_{ex} > 1.2$ T. In case of 14 K, the TF reached dip at $B_{ex} = 2$ T, mainly due to flux flow out and over magnetization. While in case of 20 K, the bulk reached saturation magnetic TF value of 0.5 T approximately at $B_{ex} = 1.4$ T. This decrease can also be supported with the TF analysis

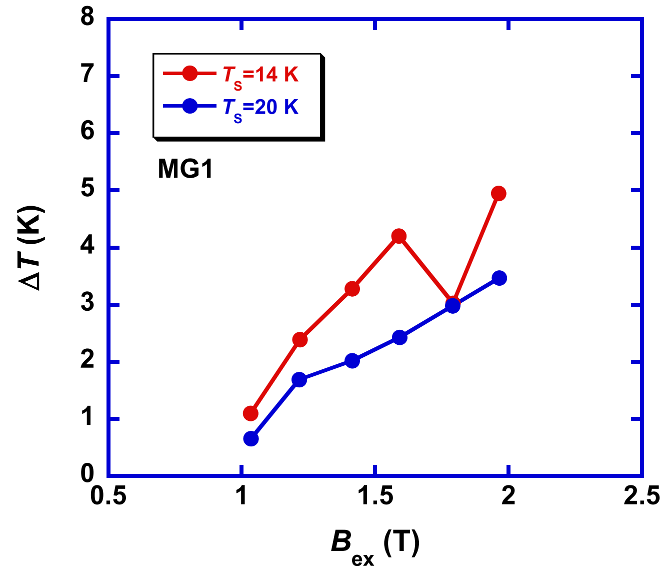

Fig. 15. Temperature dependence on the applied pulse field at 14 and 20 K.

done on Gd-Ba-Cu–O bulks, where they have observed that the trapped flux distribution may vary with increasing may vary with applied field. The trapped field had a tendency to reach a multi-peak profile due to partial flux motion when multiple pulses were used to increase the applied field. This led to TF saturation or decrease with increasing the applied peak field [36,37]. The same can be expected with the MgB_2 bulks when subjected to pulsed-field magnetization (PFM). Fig. 14 shows the total trapped flux (ϕ_T) dependence on B_{ex}, 1 mm above bulk surface. In both temperatures, 14 and 20 K, high total trapped flux was observed when $B_{ex} = 0.8$ T. In both temperatures, the trapped flux was not proportional to applied field, instead, there were dips and rises. Evidently, magnetic flux does not enter the bulk at every extra pulse uniformly. The magnetization history in an incompletely magnetized sample and the local overheating in the sample volume and the related flux loss play an important role. This behavior is not unique and has been observed also elsewhere[36]. The curves of B_T vs B_{ex} and ϕ_T vs B_{ex} for 14 and 20 K differed in the trapped field distortion in high external magnetic fields. We measured the temperature of the bulk during field application by means of a Cernox thermometer on the side of the SUS ring. The rise in temperature (ΔT) was calibrated. Fig. 15 shows the temperature during pulse field application for both 14 and 20 K. Temperature rises due to a local pinning failure, flux motion, the associated rise in electrical resistivity, local overheating and so on. The rise in electrical resistivity is a consequence of flux motion that leads to a local loss of superconductivity. The rise in resistivity is microscopic and local. The local temperature keeps rising with increase in applied pulse field. Tatsuya *et al.* [33] showed an increase of temperature with increasing applied field similar to the present work. It implies that thermal conductivity is an important issue when considering production of high trapped field MgB_2 magnets. MgB_2 does not have good thermal conductivity and it would be desirable to reinforce it by a compound high thermally conductive.

4. Conclusion

We have successfully demonstrated good trapped field properties of a SPS fabricated MgB_2 bulk. XRD measurements showed single phase MgB_2 formation with a fractional amount of MgO impurities. The M-T loops showed a sharp superconducting transition at 37.5 K. The J_c values are also high compared to regular sintered bulks. Flux pinning diagrams confirmed dominance of grain boundary pinning, with peak position at 0.2. Bending tests showed that SPS MgB_2 bulks can exhibit high bending strengths but are highly brittle. These mechanical properties correlate with high packing ratio of SPS MgB_2 bulk, close to 99.8%. Magnetization process was studied at 14 and 20 K, the stray field originating from the trapped field was measured 1 mm above the bulk's surface. At 14 K, M-shaped trapped field distribution (partial magnetized state) was observed at low applied pulse fields, while at higher applied fields (>1.6 T) a cone shaped trapped field distribution was observed (fully and over magnetized states). At 20 K, moderate applied fields (1.4–1.6 T) led to a cone shaped TF distribution and higher applied fields (>1.6 T) resulted in distorted TF profiles. At the higher applied fields, flux jumps were observed, which caused a sudden drop in local TF values. In addition, characteristic MgB_2 TF decay with time was also observed. Local trapped field B_T and model trapped field $B_{estimated}$ of SPS MgB_2 bulk were compared for two temperatures, 14 and 20 K. The rise in temperature during flux jump was proportional to the applied pulse field. To reduce unwanted flux jumps, the MgB_2 blocks need a good thermal conductive reinforcement around or soaked into. All in all, PFM is an efficient and relatively cheap method of the bulk magnetization but due to flux jumps trapped field is not simply proportional to the applied pulse and the optimum pulse value is specific for each sample size, material, and operating temperature.

Declaration of Competing Interest

The authors declare that they have no known competing financial interests or personal relationships that could have appeared to influence the work reported in this paper.

Acknowledgements

This work was partly supported by Shibaura Institute of Technology (SIT) International Research Center for Green Electronics and Grant-in-Aid FD research budget code: 721MA56383. One of the authors (SSA) acknowledges support from SIT for his post-doctoral fellowship.

References

[1] J. Nagamatsu, N. Nakagawa, T. Muranaka, Y. Zenitani, J. Akimitsu, Superconductivity at 39K in magnesium diboride, Nature 410 (2001) 63–64.

[2] S.I. Schlachter, W. Goldacker, A. Frank, B. Ringsdorf, H. Orschulko, Properties of MgB_2 superconductors with regard to space applications, Cryogenics 46 (2-3) (2006) 201–207, https://doi.org/10.1016/j.cryogenics.2005.11.003.

[3] M. Tomsic, M. Rindfleisch, J. Yue, K. McFadden, J. Phillips, M.D. Sumption, M. Bhatia, S. Bohnenstiehl, E.W. Collings, Overview of MgB 2 superconductor applications, Int. J. Appl. Ceramic Technol. 4 (3) (2007) 250–259, https://doi.org/10.1111/j.1744-7402.2007.02138.x.

[4] W. Yao, J. Bascuñán, S. Hahn, Y. Iwasa, MgB_2 coils for MRI applications, IEEE Trans. Appl. Supercond. 20 (2010) 756–759, https://doi.org/10.1109/TASC.2010.2044035.

[5] B.A. Glowacki, M. Majoros, M. Eisterer, S. Toenies, H.W. Weber, M. Fukutomi, K. Komori, K. Togano, MgB_2 superconductors for applications, Physica C 387 (1-2) (2003) 153–161, https://doi.org/10.1016/S0921-4534(03)00662-2.

[6] K. Vinod, R.G.A. Kumar, U. Syamaprasad, Prospects for MgB 2 superconductors for magnet application, Supercond. Sci. Technol. 20 (1) (2007) R1–R13, https://doi.org/10.1088/0953-2048/20/1/R01.

[7] N. Rogado, M.A. Hayward, K.A. Regan, Y. Wang, N.P. Ong, H.W. Zandbergen, J. M. Rowell, R.J. Cava, Low temperature synthesis of MgB_2, J. Appl. Phys. 91 (2002) 274–277, https://doi.org/10.1063/1.1420771.

[8] A.K. Ghosh, L.D. Cooley, A.R. Moodenbaugh, Investigation of instability in high J_c Nb_3Sn strands, IEEE Trans. Appl. Supercond. 15 (2005) 3360–3363, https://doi.org/10.1109/TASC.2005.848904.

[9] P.M. Aswathy, J.B. Anooja, P.M. Sarun, U. Syamaprasad, An overview on iron based superconductors, Supercond. Sci. Technol. 23 (7) (2010) 073001, https://doi.org/10.1088/0953-2048/23/7/073001.

[10] Y. Kamihara, H. Hiramatsu, M. Hirano, R. Kawamura, H. Yanagi, T. Kamiya, H. Hosono, Iron-based layered superconductor: LaOFeP, J. Am. Chem. Soc. 128 (2006) 10012–10013, https://doi.org/10.1021/ja063355c.

[11] A.G. Bhagurkar, A. Yamamoto, L. Anguilano, A.R. Dennis, J.H. Durrell, N. Hari Babu, D.A. Cardwell, A trapped magnetic field of 3 T in homogeneous, bulk MgB 2 superconductors fabricated by a modified precursor infiltration and growth process, Supercond. Sci. Technol. 29 (3) (2016) 035008, https://doi.org/10.1088/0953-2048/29/3/035008.

[12] K. Nagashima, T. Higuchi, J. Sok, S.I. Yoo, H. Fujimoto, M. Murakami, The trapped field of YBCO bulk superconducting magnets, Cryogenics 37 (10) (1997) 577–581.

[13] T. Naito, T. Sasaki, H. Fujishiro, Trapped magnetic field and vortex pinning properties of MgB 2 superconducting bulk fabricated by a capsule method, Supercond. Sci. Technol. 25 (9) (2012) 095012, https://doi.org/10.1088/0953-2048/25/9/095012.

[14] L. Gozzelino, R. Gerbaldo, G. Ghigo, D. Torsello, V. Bonino, M. Truccato, M. A. Grigoroscuta, M. Burdusel, G.V. Aldica, V. Sandu, I. Pasuk, P. Badica, High magnetic shielding properties of an MgB 2 cup obtained by machining a spark-plasma-sintered bulk cylinder, Supercond. Sci. Technol. 33 (4) (2020) 044018, https://doi.org/10.1088/1361-6668/ab7846.

[15] A. Murakami, H. Teshima, T. Naito, H. Fujishiro, T. Kudo, H. Fujishiro, Mechanical properties of MgB_2 bulks, Phys. Procedia. 58 (2014) 98–101, https://doi.org/10.1016/j.phpro.2014.09.034.

[16] S. Safran, Critical current density and mechanical performance of MgB2 superconductors prepared with different magnesium sources, Ceram. Int. 45 (8) (2019) 10243–10249, https://doi.org/10.1016/j.ceramint.2019.02.077.

[17] T.C. Shields, K. Kawano, D. Holdom, J.S. Abell, Microstructure and superconducting properties of hot isostatically pressed MgB 2, Supercond. Sci. Technol. 15 (2) (2002) 202–205, https://doi.org/10.1088/0953-2048/15/2/303.

[18] S.Y. Lee, S.I. Yoo, Y.W. Kim, N.M. Hwang, D.Y. Kim, Preparation of Dense MgB2 Bulk Superconductors by Spark Plasma Sintering, J. Am. Ceram. Soc. 86 (2003) 1800–1802. doi:10.1111/j.1151-2916.2003.tb03559.x.

[19] J.G. Noudem, M. Aburras, P. Bernstein, X. Chaud, M. Muralidhar, M. Murakami, Development in processing of MgB 2 cryo-magnet superconductors, J. Appl. Phys. 116 (16) (2014) 163916, https://doi.org/10.1063/1.4900725.

[20] M. Muralidhar, K. Nozaki, H. Kobayashi, X.L. Zeng, A. Koblischka-Veneva, M. R. Koblischka, K. Inoue, M. Murakami, Optimization of sintering conditions in bulk MgB_2 material for improvement of critical current density, J. Alloy. Compd. 649 (2015) 833–842, https://doi.org/10.1016/j.jallcom.2015.07.191.

[21] C.P. BEAN, Magnetization of High-Field Superconductors, Rev. Mod. Phys. 36 (1) (1964) 31–39.

[22] D. Dew-Hughes, Flux pinning mechanisms in type II superconductors, Phil. Mag. 30 (2) (1974) 293–305.

[23] V. Zablotskii, M. Jirsa, P. Petrenko, Phys. Rev. B 65 (2002) 2245081-4. doi: 10.1103/PhysRevB.65.224508.

[24] M. Jirsa M. Rameš, M. Miryala, P. Svora, J. Duchon, O. Molnarova, S.S. Arvapalli, M. Murakami, Supercond. Sci. Technol. 33 (2020) 094007 (1–8) doi:10.1088/1361-6668/aba01c.

[25] S.S. Arvapalli, M. Miryala, M. Jirsa, M. Murakami, A. Sai Srikanth, M. Muralidhar, J. Milos, M. Murakami, Size reduction of boron particles by high-power ultrasound for optimization of bulk MgB_2, Supercond. Sci. Technol. 33 (2020), 115009, https://doi.org/10.1088/1361-6668/abb63e.

[26] M. Miryala, S.S. Arvapalli, P. Diko, M. Jirsa, M. Murakami, Flux pinning and superconducting properties of bulk MgB 2 with MgB 4 addition, Adv. Eng. Mater. 22 (3) (2020) 1900750, https://doi.org/10.1002/adem.201900750.

[27] S.S. Arvapalli, M. Muralidhar, M. Murakami, High-performance bulk MgB_2 superconductor using amorphous nano-boron, J Supercond Nov Magn 32 (7) (2019) 1891–1895, https://doi.org/10.1007/s10948-018-4919-x.

[28] M. Jirsa, M. Rames, M.R. Koblischka, A. Koblischka-Veneva, K. Berger, B. Douine, Relaxation and pinning in spark-plasma sintered MgB 2 superconductor, Supercond. Sci. Technol. 29 (2) (2016) 025006, https://doi.org/10.1088/0953-2048/29/2/025006.

[29] M.P. Anderson, D.J. Srolovitz, G.S. Grest, P.S. Sahni, Computer simulation of grain growth—I. Kinetics, Acta Metall. 32 (5) (1984) 783–791, https://doi.org/10.1016/0001-6160(84)90151-2.

[30] J.H. Durrell, A.R. Dennis, J. Jaroszynski, M.D. Ainslie, K.G.B. Palmer, Y.-H. Shi, A. M. Campbell, J. Hull, M. Strasik, E.E. Hellstrom, D.A. Cardwell, A trapped field of 17.6 T in melt-processed, bulk Gd-Ba-Cu-O reinforced with shrink-fit steel, Supercond. Sci. Technol. 27 (8) (2014) 082001, https://doi.org/10.1088/0953-2048/27/8/082001.

[31] A. Murakami, A. Iwamoto, J.G. Noudem, Mechanical properties of bulk MgB_2 superconductors processed by spark plasma sintering at various temperatures, IEEE Trans. Appl. Supercond. 28 (3) (2018) 1–4.

[32] M. Muralidhar, K. Inoue, M.R. Koblischka, M. Tomita, M. Murakami, Optimzation of processing condiations towards high trapped fields in MgB_2 bulk, J. Alloy. Compd. 608 (2014) 102–109.

[33] T. Hirano, Y. Takahash, S. Namba, T. Naito, H. Fujishiro, A record-high trapped field of 1.61 T in MgB_2 bulk comprised of copper plates and soft iron yoke cylinder using pulsed-field magnetization, Supercond. Wires Basics Appl. 33 (2020) 10.

[34] H. Fujishiro, T. Hiyama, T. Tateiwa, Y. Yanagi, T. Oka, Importance of initial "M-shaped" trapped field profile in a two-stage pulse field magnetization (MMPSC) method, Physica C (Amsterdam, Neth.) 463-465 (2007) 394–397, https://doi.org/10.1016/j.physc.2007.03.440.

[35] S. Zou, V.M.R. Zermeño, A. Baskys, A. Patel, F. Grilli, B.A. Glowacki, Simulation and experiments of stacks of high temperature superconducting coated conductors magnetized by pulsed field magnetization with multi-pulse technique, Supercond. Sci. Technol. 30 (1) (2017) 014010, https://doi.org/10.1088/0953-2048/30/1/014010.

[36] M.D. Ainslie, J. Srpcic, D. Zhou, H. Fujishiro, K. Takahashi, D.A. Cardwell, J. H. Durrell, Toward optimization of multi-pulse, pulsed field magnetization of bulk high-temperature superconductors, IEEE Trans. Appl. Supercond. 28 (4) (2018) 1–7, https://doi.org/10.1109/TASC.2017.2788924.

[37] T. Ida, H. Matsuzaki, Y. Akita, M. Izumi, H. Sugimoto, Y. Hondou, Y. Kimura, N. Sakai, S. Nariki, I. Hirabayashi, M. Miki, M. Murakami, M. Kitano, Magnetization properties for Gd–Ba–Cu–O bulk superconductors with a couple of pulsed-field vortex-type coils, Physica C 412-414 (2004) 638–645, https://doi.org/10.1016/j.physc.2003.12.082.